Bottom-up Nanofabrication of Crystalline Structures of Magnetic Nanoparticles

Xiaozheng Xue[1] and Edward P. Furlani[1, 2]

1 Dept. of Chemical and Biological Engineering, University at Buffalo SUNY,
Email:xiaozhen@buffalo.edu
2 Dept. of Electrical Engineering, University at Buffalo SUNY,
Office: (716) 645-1194 Fax: (716) 645-3822, Email:efurlani@buffalo.edu

ABSTRACT

A bottom-up approach to the nanofabrication of three-dimensional (3D) crystalline structures of magnetic core-shell nanoparticles is presented. The approach is based on self-assembly and involves the use of soft-magnetic template elements to guide the assembly in the presence of a uniform bias field. The combination of a bias field and template-induced gradient fields provides localized regions of attractive and repulsive magnetic force that enable nanoscale control of particle placement during assembly. The method is demonstrated using a computational model that predicts particle dynamics during assembly and the final assembled structure. The analysis demonstrates that 3D crystalline superstructures can be assembled within milliseconds and that the feature resolution of the assembled structure can be tailored by controlling the process variables. This method of nanofabrication opens up opportunities for the scalable fabrication of nanostructured materials with unprecedented properties for a broad range of applications.

Keywords: Magnetic field-directed self-assembly of core-shell nanoparticle structures, template-assisted self-assembly of magnetic core-shell nanoparticles, bottom up nanofabrication, Langevin dynamics, magnetic dipole-dipole interactions.

1 INTRODUCTION

The interest in the field-directed control of magnetic particles has grown steadily in recent years due to rapid advances in particle synthesis and related enabling technologies [1-4]. Applications in this field include gene transfection [5,6], drug delivery [7,8], microfluidic-based bioseparation [9] and sorting [10]. Researchers have also explored the use of magnetic paticles' self-assembly to enable a bottom-up approach for the scalable fabrication of nanostructured materials, e.g. for photonic [11,12], magnetic, micro-optical [13] and electronic applications [14,15]. Such an approach would open up opportunities for the low-cost high-throughput production of functional nanocomposite materials.

In this presentation we demonstrate a method for controlling the self-assembly of colloidal magnetic core-shell nanoparticles into extended 3D crystalline superstructures. In this method, submicron (e.g. lithographically-patterned) template elements are used to achieve nanoscale resolution in particle placement. The templates are made from a soft-magnetic material (e.g. Permalloy, a nickel-iron alloy) and are embedded in a nonmagnetic substrate. A uniform bias field is applied to magnetize the template elements. **Fig.1** shows a portion of a self-assembly system that consists of a nonmagnetic substrate with a periodic 2D array of embedded cylindrical template elements. To achieve assembly, colloidal particles in suspension are first deposited onto the substrate in the absence of an external magnetic field. A uniform external field is then applied that saturates the soft-magnetic template elements to generate a magnetic gradient field that drives the self-assembly process. We use a computational model to study the detailed dynamics of the assembly process.

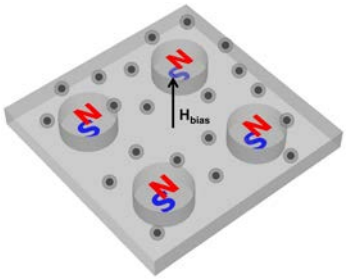

Fig.1 A template-assisted self-assembly system showing colloidal core-shell nanoparticles above a nonmagnetic substrate that contains an array of embedded soft-magnetic cylindrical template elements.

2 COMPUTATIONAL MODEL

The behaviour of colloidal magnetic particles in an applied field depends on a number of factors including hydrodynamic and magnetic forces, Brownian motion, Van der Walls force and the effects of surfactants. We predict the self-assembly of such particles using a computational model based on Langevin's equation that takes these effects into account,

$$m_i \frac{d^2 \boldsymbol{x}_i}{dt^2} = \boldsymbol{F}_{mag,i} + \boldsymbol{F}_{vis,i} + \boldsymbol{F}_{B,i}(t) + \sum_{\substack{j=1 \\ j\neq i}}^{N} \left(\boldsymbol{F}_{dd,ij} + \boldsymbol{F}_{vdw,ij} + \boldsymbol{F}_{surf,ij} + \boldsymbol{F}_{hyd,ij} \right), \quad (1)$$

Where m_i and $x_i(t)$ are the mass and position of the i'th particle. The right-hand-side of this equation represents the sum of forces on the i'th particle: $\boldsymbol{F}_{mag,i}$ due to the applied magnetic field, which is a superposition of the bias field and induced gradient-fields; $\boldsymbol{F}_{vis,i}$, viscous drag due to relative motion between the particles and the surrounding fluid

(Stokes drag); $\boldsymbol{F}_{B,i}(t)$ a stochastic force to account for Brownian motion; $\boldsymbol{F}_{dd,ij}$ the interparticle magnetic dipole-dipole force due to induced dipole moments; $\boldsymbol{F}_{vdw,ij}$ Van der Waals force; $\boldsymbol{F}_{surf,ij}$ a repulsive force due to surfactant contact between particles and $\boldsymbol{F}_{hyd,ij}$ due to interparticle hydrodynamic interactions. We predict the particle dynamics by numerically integrating Eq.(1) using an adaptive time stepping method to accelerate and stabilize the computation. The various terms in the model are briefly described in the following sections.

2.1 Magnetic force

The magnetic force is computed using an "effective" dipole moment method in which the particle is modeled as an "equivalent" point dipole with an effective moment $\boldsymbol{m}_{eff}$. The force on the i'th particle is given by [16]

$$\boldsymbol{F}_{mag,i} = \mu_f \left(\boldsymbol{m}_{i,eff} \cdot \nabla\right) \boldsymbol{H}_a , \quad (2)$$

where μ_f is the permeability of the fluid and H_a is the applied magnetic field intensity at the center of particlee [16,17].

2.2 Magnetic dipole-dipole interaction

The potential energy for magnegic dipoles is given by

$$U_{dd,ij} = -\frac{\mu_f}{4\pi}\left(3\frac{\left(\boldsymbol{m}_{i,eff}\cdot\boldsymbol{r}_{ij}\right)\left(\boldsymbol{m}_{j,eff}\cdot\boldsymbol{r}_{ij}\right)}{r_{ij}^5} - \frac{\boldsymbol{m}_{i,eff}\cdot\boldsymbol{m}_{j,eff}}{r_{ij}^3}\right), \quad (3)$$

where $\boldsymbol{m}_{i,eff}$ and $\boldsymbol{m}_{j,eff}$ are the moments of i'th and j'th particle, respectively, and $\boldsymbol{r}_{ij}$ is the displacement vector between them. The dipole-dipole force in Eq.(1) is obtained as the gradient of the potential,

$$\boldsymbol{F}_{dd,ij} = -\nabla U_{dd,ij} . \quad (4)$$

2.3 Van der Waals interaction

Van der Waals force is given by [18],

$$\boldsymbol{F}_{vdw,ij} = \frac{32A}{3}\frac{(R_{p,i}\cdot R_{p,j})^3 \cdot r_{ij}}{(r_{ij}^2-(R_{p,i}+R_{p,j})^2)^2\cdot(r_{ij}^2-(R_{p,i}-R_{p,j})^2)^2}, \quad (5)$$

where A is the Hamaker constant and h_{ij} is the surface-to-surface separation distance between the i'th and j'th particle.

2.4 Surfactant force

The repulsive force caused by surfactant-surfactant contact is modelled using

$$\boldsymbol{F}_{rep,ij} = -\nabla U_s = \frac{16\pi N_s k_b T}{\delta_i+\delta_j}\frac{R_{p,i}^2 R_{p,j}^2}{(R_{p,i}+R_{p,j})^2}\ln\left(\frac{R_{p,i}+R_{p,j}}{r_{ij}}\right), \quad (6)$$

where R_p, δ and N_s are, respectively, the radius of particle, the thickness of the surfactant layer and the surface density of surfactant molecules [19].

2.5 Viscous drag

The viscous drag on a particle is computed using Stokes' formula

$$\boldsymbol{F}_{D,i} = D\frac{d\boldsymbol{x}_i}{dt}, \quad (7)$$

where $D = 6\pi\eta R_{hyd,p}$ is the drag coefficient, η is the fluid viscosity and $R_{hyd,p}$ is the hydrodynamic radius of the particle.

2.6 Interparticle hydrodynamics interactions

Interparticle hydrodynamic interactions are taken into account using lubrication theory, with a force of the form [18],

$$\boldsymbol{F}_{lub,ij} = \frac{6\pi\mu_f \boldsymbol{V}_{r,i,j}}{h_{ij}}\frac{R_{p,i}^2 R_{p,j}^2}{(R_{p,i}+R_{p,j})^2}, \quad (8)$$

where h_{ij} is the separation bewteen the surfaces and $\boldsymbol{V}_{r,i,j}$ is the relative velocity between the particles.

2.7 Brownian diffusion

The Brownian force was modeled as a Gaussian white noise process. The magnitde of this force in one dimension is

$$\boldsymbol{F}_{B,i}(t) = \xi\sqrt{\frac{2Dk_BT}{\Delta t}} \quad (9)$$

where is Boltzmann's constant, D is is the Stokes' drag coefficient as described above and ξ is a random number with a Gaussian distribution.

2.8 Equations of Motion

Particle motion during assembly is predicted by solving Langevin's equation,

$$m_i\frac{d^2\boldsymbol{x}_i}{dt^2} + D\frac{d\boldsymbol{x}_i}{dt} = \boldsymbol{F}_{sum,i}, \quad (10)$$

where

$$\boldsymbol{F}_{sum,i} = \boldsymbol{F}_{mag,i} + \boldsymbol{F}_{B,i}(t) + \sum_{\substack{j=1\\ j\neq i}}^{N}\left(\boldsymbol{F}_{dd,ij}+\boldsymbol{F}_{vdw,ij}+\boldsymbol{F}_{rep,ij}+\boldsymbol{F}_{lub,ij}\right), \quad (11)$$

Eq. (10) is solved after reduction to coupled first-order system of equations,

$$\Delta\boldsymbol{x}_i = \frac{\boldsymbol{F}_{sum,i}}{D}\tau + \frac{m_i}{D}\left(\boldsymbol{v}_{i,0} - \frac{\boldsymbol{F}_{sum,i}}{D}\right)\left(1\text{-}e^{-\frac{D}{m_i}\tau}\right), \quad (12)$$

$$\boldsymbol{v}_{i,f} = \frac{\boldsymbol{F}_{sum,i}}{D} + \left(\boldsymbol{v}_{i,0} - \frac{\boldsymbol{F}_{sum,i}}{D}\right)e^{-\frac{D}{m_i}\tau}, \quad (13)$$

that are integrated using a numerical time-stepping scheme.

3 RESULTS

We have used the model to study the system that consists of soft-magnetic cylinders that are embedded in a non-magnetic substrate **Fig. 1**. A uniform bias field $\boldsymbol{H}_{bias}$ is applied perpendicular to the substrate to magnetize the elements. We study the self-assembly of Fe_3O_4-SiO_2 core-shell particles with a core diameter of 17 nm ($R_{core} = 8.5\,nm$) and a shell thickness of 11.5 nm. The template elements are permalloy (78% Ni, 22% Fe), which has a saturation magnetization $M_{e,s} = 8.6\times10^5\ A/m$. The bias field is taken to be $H_{bias} = 3.9\times10^5\ A/m$ ($B_{bias} = 5000\ Gauss$), which is sufficiently strong to saturate both the nanoparticles and the template elements. Their hydrodynamic radius is assumed to be the same as their

physical radius $R_{hyd,p} = 40\,nm$. The carrier fluid is assumed to be nonmagnetic with a viscosity and density equal to that of water.

We use field and force equations from our previous work [20-21] to compute the radial and axial magnetic field and force components as shown in **Fig.2**. We choose the radius and height of soft-magnetic cylindrical temple to be $R_m = 200\,nm$ and $h = 300\,nm$, which has a demagnetization factor as 0.46. Thus, a uniform external bias field (0.5 T) will be applied to saturate the soft-magnetic elements, which ensures that $\boldsymbol{H}_{bias} \geq N_d \boldsymbol{M}_{es}$. The spacing between the elements is taken to be 2 μm center-to-center so that there is negligible overlap of their fields. The radial and axial force components $F_{mag,r}$ and $F_{mag,z}$ are computed at a distance $z = 100\,nm$ above the template geometry as shown in **Fig. 2c** and **d**. The analysis shows that there is a relatively strong attractive axial force over the center of the element, $r/R_m < 1$, which promotes assembly in this region. There is also a relatively weak repulsive (upward-directed) axial force above near the exterior edge of cylinder ($r = R_m$) that prevents particles from assembling there. Note from **Fig. 2c** that this force component peaks (in a negative sense) above the radial edge of the element and therefore acts to move the particles inward towards the center of the element.Thus, the magnetic force directs particles towards the center of the template during assembly, which promotes the formation of a tapered 3D pyramid structure. The ability to produce regions of attractive and repulsive magnetic force is a key feature of the proposed assembly method that enables nanoscale precision of particle placement.

Next, we use the computational model to study the dynamics of the assembly process. The bias field and template dimensions are as above. We use a computational domain centered with respect to a single element. The

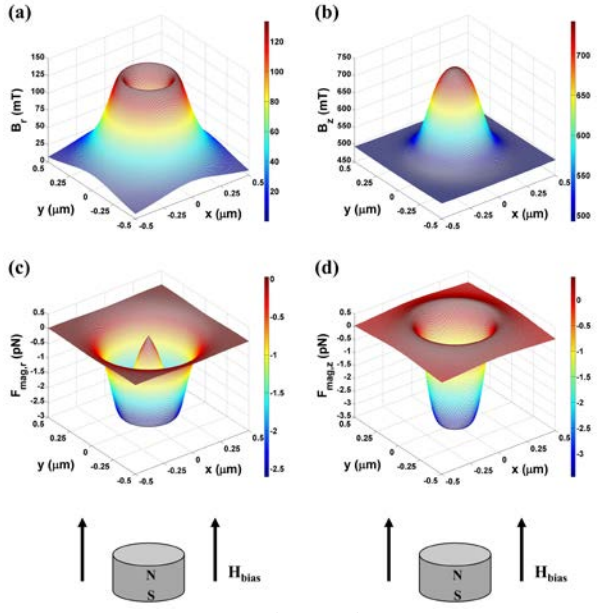

Fig.2 Axisymmetric magnetic field and force components at z=100 nm above the template element: (a) Br, (b) Bz, (c) Fmag,r, and (d) Fmag,z

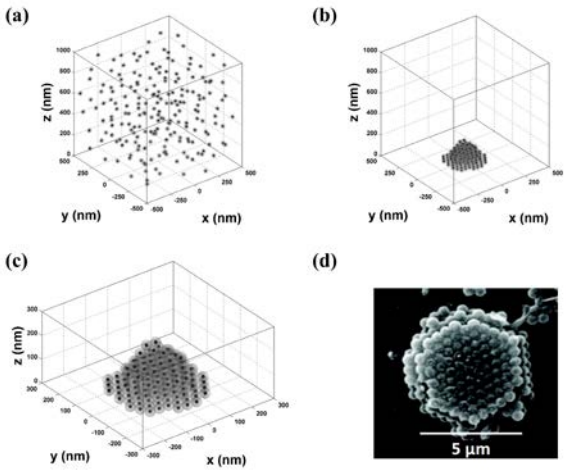

Fig. 3 Initial and final particle distributions for a cylindrical template element: (a) initial random particle distribution, (b) perspective of final assembled particle structure, (c) lateral view of assembled particle structure, (d) field-directed assembly of non-magnetic beads in a ferrofluid using cylindrical traps [22].

domain spans a unit cell, i.e. 1 μm along both the *x* and *y* axes and 1 μm in the *z*-direction as shown in **Figs. 3a**. The base of the domain is at $z = 0$, which coincides with the top surface of both the substrate and the template element. Periodic boundary conditions for particle transport are imposed at the lateral sides of the domain to account for a 2D array of template elements. We simulate the assembly of 40 *nm* Fe_3O_4-SiO_2 particles with a 17 nm Fe_3O_4 core. Note that the assembled structure shown in **Fig 3c** has a uniform hcp crystalline structure that is tapered due to focusing by the magnetic force as described above. This structure is very similar to those observed by Yellen et al. as shown in **Fig. 3d**[22**]**. The individual colored-coded layers in the

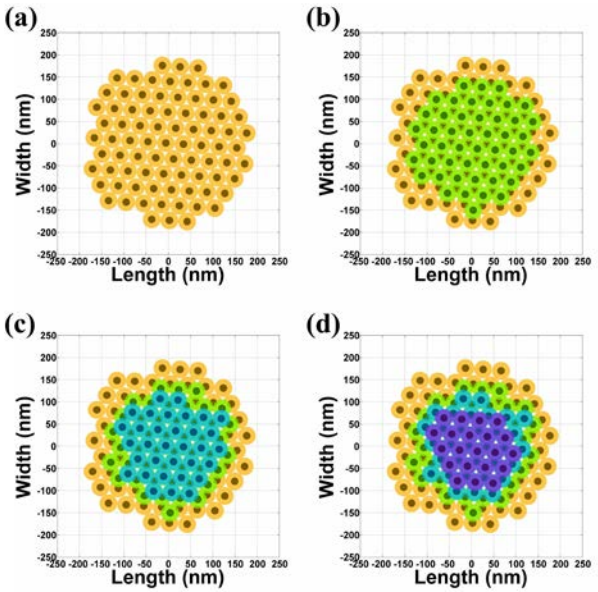

Fig. 4 Multi-layer hexagonal packed structure. (a), (b), (c) and (d) are indicated as 1st, 2nd, 3rd and 4th layer of the particles' structure after assembly. The particle core is shown as a solid sphere and the shell is

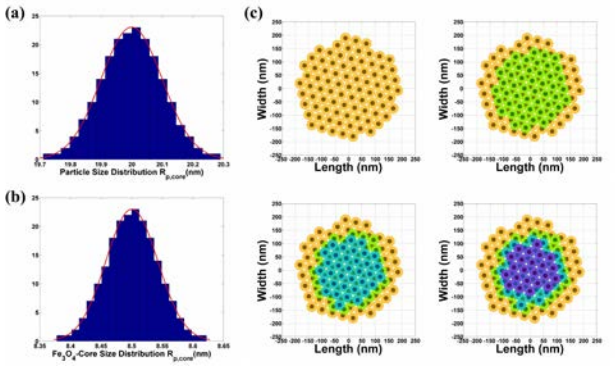

Fig. 5 Multi-layer hexagonal packed structure for a cylindrical template element with particle size distribution: (a) particle size distribution, (b) Fe3O4 core size distribution, (c) 4 layers' hexagonal packed structure after assembly.

assembled structure are shown in **Fig. 4**. Note that there are no defects (i.e. interparticle gaps) in these layers. However, as the number of partice layers increases, defects in crystalline structure can occur, which are due to a decrease in effect of the gradient field force that tends to pack the particles.

Next, we study the effcet of a size distribution on the self-assembly process. We consider a polydisperse system of core-shell particles that is based on a Gaussian size distribution as shown in **Fig.5a** and **b**. The oveall particle size varies between 19.7 nm and 20.3 nm, while the core size varies between 8.3 nm and 8.7 nm, as shown in **Fig.5a** and **b**. As shown in **Fig 5c** the assembled structure has a uniform hcp crystalline structure that is similar to the monodisperse system. However, our works show that as the size distribution increases, defects occur in the crystalline structure.

4 CONCLUSIONS

We have described a method for directing the assembly of colloidal magnetic-dielectric core-shell nanoparticles into extended 3D crystalline structures with nanoscale precision. In this method, sub-micron soft-magnetic template elements are used to guide the assembly in the presence of a uniform bias field. The use of a uniform bias field combined with localized high gradient fields produced by the template elements is a key feature of the method that enables nanoscale precision of particle placement, which translates to nanoscale feature resolution in the assembled structure. We have demonstrated proof-of-concept of the method using a computational model that takes into account the dominant assembly mechanisms. The method broadly applies to arbitrary template geometries and multi-layered particles with at least one magnetic component. The ability to produce such materials opens up opportunities for the scalable high-throughput fabrication of multifunctional nanostructured materials for a broad range of applications and our computational model enables the rational design of such media.

ACKNOWLEDGEMENTS

The authors acknowledge financial support from the U.S. National Science Foundation, through award number CBET-1337860.

REFERENCES

[1] Pankhurst, Q.A.; Thanh, N.K.T.; Jones, S.K.; Dobson, J. Progress in applications of magnetic nanoparticles in biomedicine. In J. Phys. D Appl. Phys., 2009, 42(22), 224001/224001-224001/224015.

[2] Pamme, N. Magnetism and microfluidics. In Lab Chip, 2006, 6(1), 24-38.

[3] Berry, C.C. Progress in functionalization of magnetic nanoparticles for applications in biomedicine. In J. Phys. D Appl. Phys., 2009, 42(22), 224003/224001-224003/224009.

[4] Furlani, E.P. Magnetic biotransport: analysis and applications. In Materials, 2010, 3, 2412-2446.

[5] Dobson, J. Gene therapy progress and prospects: magnetic nanoparticle-based gene delivery. In Gene Ther., 2006, 13(4), 283-287.

[6] Furlani, E.P.; Xue, X. Field, force and transport analysis for magnetic particle-based gene delivery. In Microfluid. Nanofluid., 2012, 13(4), 589-602.

[7] Furlani, E.P.; Xue, X. A Model for Predicting Field-Directed Particle Transport in the Magnetofection Process. In Pharm. Res., 2012, 29(5), 1366-1379.

[8] Arruebo, M; Fernández-Pacheco, R; Ibarra, M.R; Santamaría, J. Magnetic nanoparticles for drug delivery. In Nanotoday, 2007, 2(3):22–32.

[9] Ganguly, R.; Puri, I.K. Microfluidic transport in magnetic MEMS and bioMEMS. In Wiley Interdiscip. Rev. Nanomed. Nanobiotechnol., 2010, 2(4), 382-399.

[10] Zborowski, M; Chalmers J.J. Magnetic cell separation, vol 32 (Laboratory techniques in biochemistry and molecular biology). In Elsevier Science, 2007, New York.

[11] Yethiraj, A.; Thijssen, J.H.J.; Wouterse, A.; Van Blaaderen, A. Large-area electric-field-induced colloidal single crystals for photonic applications. In Adv. Mater. (Weinheim, Ger.), 2004, 16(7), 596-600.

[12] Xia, Y.; Gates, B.; Li, Z.-Y. Self-assembly approaches to three-dimensional photonic crystals. In Adv. Mater. (Weinheim, Ger.), 2001, 13(6), 409-413.

[13] Lu, Y.; Yin, Y.; Xia, Y. A self-assembly approach to the fabrication of patterned, two-dimensional arrays of microlenses of organic polymers. In Adv. Mater. (Weinheim, Ger.), 2001, 13(1), 34-37.

[14] Shipway, A.N.; Katz, E.; Willner, I. Nanoparticle arrays on surfaces for electronic, optical, and sensor applications. In ChemPhysChem, 2000, 1(1), 18-52.

[15] Hochbaum, A.I.; Fan, R.; He, R.; Yang, P. Controlled growth of Si nanowire arrays for device integration. In Nano Lett., 2005, 5(3), 457-460.

[16] Furlani, E.P. Analysis of particle transport in a magnetophoretic microsystem. In J. Appl. Phys., 2006, 99(2), 024912/024911-024912/024911.

[17] Furlani, E.P.; Ng, K.C. Nanoscale magnetic biotransport with application to magnetofection. In Phys. Rev. E Stat., Nonlinear, Soft Matter Phys., 2008, 77(6-1), 061914/061911-061914/061918.

[18] Russel, W.B.; Saville, D.A.; Schowalter, W.R., Colloidal Dispersions, Cambridge University Press, 1989.

[19] Rosensweig, R.E. Fluid dynamics and science of magnetic liquids. In Advances in Electronics and Electron Physics. 1979, Vol. 48: Martin M (ed.) Academic Press, New York, pp. 103-99.

[20] Xue, X.; Furlani, E.P. Template-assisted nano-patterning of magnetic core–shell particles in gradient fields. Physical Chemistry Chemical Physics, 2014, 16(26), 13306-13317.

[21] Xue, X.; Furlani, E.P. Analysis of the Dynamics of Magnetic Core-shell Nanoparticles and Self-assembly of Crystalline Superstructures in Gradient Fields. The Journal of Physical Chemistry C, 2015.

[22] Yellen, B.B.; Hovorka, O.; Friedman, G. Arranging matter by magnetic nanoparticle assemblers. Proceedings of the National Academy of Sciences of the United States of America, 2005, 102(25), 8860-8864.